

# Molecular-Scale Exploration of Mechanical Properties and Interactions of Poly(lactic acid) with Cellulose and Chitin

Paulo G. M. Mileo,\* Caroline M. Krauter, Jeffrey M. Sanders, Andrea R. Browning,\* and Mathew D. Halls



Cite This: *ACS Omega* 2023, 8, 42417–42428



Read Online

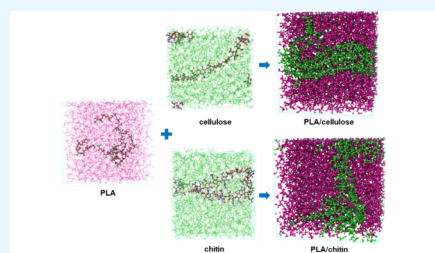
ACCESS |

Metrics & More

Article Recommendations

Supporting Information

**ABSTRACT:** Poly(lactic acid) (PLA), one of the pillars of the current overarching displacement trend switching from fossil- to natural-based polymers, is often used in association with polysaccharides to increase its mechanical properties. However, the use of PLA/polysaccharide composites is greatly hampered by their poor miscibility, whose underlying nature is still vastly unexplored. This work aims to shed light on the interactions of PLA and two representative polysaccharide molecules (cellulose and chitin) and reveal structure–property relationships from a fundamental perspective using atomistic molecular dynamics. Our computational strategy was able to reproduce key experimental mechanical properties of pure and/or composite materials, reveal a decrease in immiscibility in PLA/chitin compared to PLA/cellulose associations, assert PLA-oriented polysaccharide reorientations, and explore how less effective PLA-polysaccharide hydrogen bonds are related to the poor PLA/polysaccharide miscibility. The connection between the detailed chemical interactions and the composite behavior found in this work is beneficial to the discovery of new biodegradable and natural polymer composite mixtures that can provide needed performance characteristics.



Polysaccharides cellulose and chitin in association with PLA.

## INTRODUCTION

In response to growing environmental and safety challenges as well as governmental regulations and incentives, policymakers and industry stakeholders are steadily spearheading the replacement of conventional fossil-based polymers for biodegradable and renewable materials.<sup>1–3</sup> Poly(lactic acid) (PLA), a polyester product of (L- and/or D-)lactide, is one of the leading materials in this transition, since it combines good end-product features (e.g., thermoplasticity, high-strength/modulus, and low-temperature processability) with an eco-friendly nature due to its biocompatibility, renewable sources (e.g., corn, rice), recyclability, and benign degradation.<sup>4</sup> Therefore, PLA has been applied in various industrial sectors such as packaging, fibers and textiles, automotive, pharmaceutical, and medical industries.<sup>5,6</sup> However, its application range is still limited by some of its mechanical properties, such as inherent brittleness, poor impact strength, and low thermal stability.<sup>4,7,8</sup>

Diverse alternatives have been employed in the last decades to enhance the toughness of PLA and achieve more balanced mechanical properties in this material, including plasticization, blending with other (bio)polymers, copolymerization, and incorporation of fillers.<sup>7</sup> Polysaccharides such as cellulose and chitin have been considered as viable alternatives to enhance PLA toughness because of their mechanical properties (e.g., biodegradability and high strength), affordability, and bioavailability.<sup>8,9</sup> Due to their underlying hydrophilicity, this class of materials also promotes the PLA's hydrolytic degradation, thus

rendering it more biodegradable.<sup>10</sup> However, PLA association with polysaccharides is severely hampered by their poor compatibility, partially remediated with several strategies, including aspect ratio modification,<sup>11</sup> blending with plasticizing agents,<sup>12</sup> interphase cross-linking,<sup>13</sup> and surface modification.<sup>14</sup> Molecular simulation techniques offer a powerful toolset in the effort of PLA compatibilization with other biorelevant matrices by allowing the derivation of bottom-up structure–property relationships from nanoscopic insights. For instance, atomistic and mesoscopic molecular dynamics (MD) simulations have been employed in the prediction and rationalization of the miscibility and/or mechanical properties of PLA blends with poly(styrene) and poly(vinylphenol),<sup>15</sup> poly(styrene-co-vinylphenol),<sup>16</sup> poly(hydroxybutyrate),<sup>17</sup> poly(butylene succinate),<sup>18</sup> poly( $\epsilon$ -caprolactone),<sup>19</sup> and poly(ethylene glycol).<sup>20</sup>

Naturally, MD simulations have also been instrumental in the characterization of PLA blends with polysaccharides. Particular attention has been devoted to the characterization of PLA blends with unmodified<sup>21</sup> and functionalized<sup>22,23</sup> cellulose nanocrystals (CNC). Such focus on CNC-containing PLA composites is clearly justified by the superior mechanical

**Received:** July 7, 2023

**Revised:** October 10, 2023

**Accepted:** October 13, 2023

**Published:** October 31, 2023



characteristics of pristine CNC,<sup>24</sup> despite its poor miscibility with PLA. However, it has been shown that, due to better interphase interactions, both the mechanical properties (e.g., tensile strength and elongation) and hydrolytic degradation properties of PLA/cellulose composite samples are improved when amorphous cellulose is employed in lieu of traditional crystalline samples.<sup>25</sup> Recent computational work<sup>26</sup> complements this finding by shedding light on the role of cellulose rearrangement on the improvement of the tensile properties of cellulose-containing PLA formulations. Still, much less consideration has been given to other important polysaccharide associations with PLA, such as chitin and chitosan.

In this work, using advanced MD workflows, we aim at bridging this gap and expanding the fundamental knowledge of polysaccharide/PLA associations by (i) investigating their mutual orientation and bulk organization, (ii) explaining important mechanical properties such as elastic constants, tensile strength, and glass transition temperature at the molecular level, and (iii) exploring the role of intermolecular interactions on the final properties of amorphous cellulose- and chitin-containing PLA formulations.

## MATERIALS AND METHODS

PLA, cellulose, and chitin structure models were created considering polymeric chains with degrees of polymerization of 50 and 20, respectively, and terminated with hydroxyl groups (see Figure 1). These degrees of polymerization were chosen

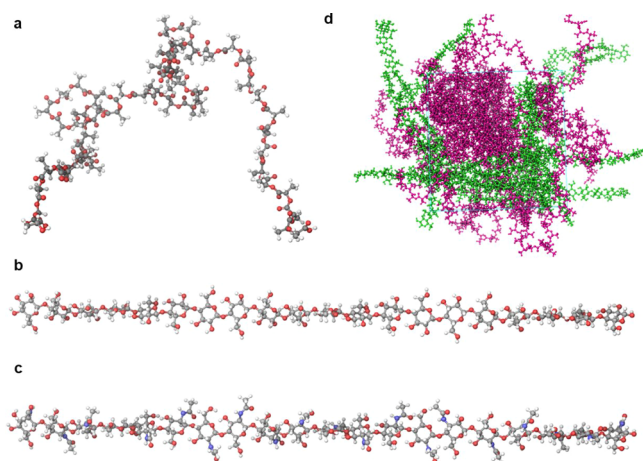


**Figure 1.** Molecular models employed in the representation of PLA (a), cellulose (b), and chitin (c). Example of an MD-equilibrated molecular model of a cellulose/PLA (respectively in green and pink) system (d). C, O, H, and N atoms are, respectively, represented in gray, red, hydrogen, and blue colors.

considering the trade-off between computational efficiency and representability of the entanglement and mechanical properties of polymers. These values were also based on previous dedicated studies and deemed adequate to represent several experimental properties of the polymers studied herein.<sup>26–29</sup>

To investigate the influence of different polysaccharide concentrations on the mechanical properties and hydrophilicity of PLA matrices, we selected five sets of cellulose- and chitin-containing PLA composites with different concentrations summarized in Table 1. As performed in previous literature work,<sup>26</sup> we study a large range of molar polysaccharide proportions in these composites, maintaining

**Table 1. Polysaccharide Content and Number of Chains of Each Component in PLA/Polysaccharide Microscopic Models**

polysaccharide content (mol %)	number of chains	
	PLA	polysaccharides
0	20	0
20	20	5
36	18	10
48	16	15
100	0	20

PLA as the main component. We considered equal amounts of PLA chains in the L and D configurations.

Schrödinger Materials Science Suite, version 21-4<sup>30</sup> was used for all models and simulations. PLA, cellulose, and chitin structure models were randomly positioned in periodic simulation boxes using the random walk (Tangled Chain) scheme of the Disordered System Builder having an initial density of 0.5 g/cm<sup>3</sup>. Using this construction scheme, we ignored crystalline or semicrystalline organizations and instead considered all systems as fully amorphous.

The OPLS4 force field,<sup>31</sup> including atomic point charges, and van der Waals parameters as well as bonded interaction terms was used. The force field has been shown to be accurate in predicting the thermal properties of a large chemical space of polymeric structures including polysaccharides.<sup>32,33</sup> Molecular dynamics (MD) simulations using the GPU-accelerated Desmond engine<sup>34,35</sup> were used to relax the constructed systems and perform property calculations. Dispersive interactions were limited to a cutoff of 9 Å radius while electrostatic interactions were calculated using the U-series treatment.<sup>36</sup>

For each polymeric system considered, 10 replicates with different initial atomic configurations were generated to improve statistics of the calculated polymer's properties. These systems were initially relaxed with a sequence of a 20 ps Brownian minimization in the canonical ensemble (NVT) at 10 K, a 20 ps Brownian minimization in the isothermal–isobaric ensemble (NPT) at 100 K, and a 100 ps MD run in the NPT ensemble with a 1 fs time step using the Nose–Hoover chain thermostat<sup>37,38</sup> and the Martyna–Tobias–Klein (MTK) barostat<sup>39</sup> with respective relaxation times of 1 and 2 ps. To further equilibrate these systems, they were annealed to a molten/amorphous state (above their glass transition temperature) at 800 K for 5 ns followed by a cooling ramp at a 2 K/ns rate until 300 K. These configurations were then used as input for final production MD simulations in the NPT ensemble at 300 K and 1.013 bar for 20 ns with a 2 fs time step. Such simulation times are significantly longer than the ones regularly employed in the literature,<sup>26,40–42</sup> however, to ensure that the equilibrium stage had been reached during these runs, we analyzed the density evolution with time for each simulation. As reported in Figure S1, we can observe that equilibrium is reached within the first nanosecond of simulation.

From the equilibrium stage of these production simulations, several primary properties such as density, molar volume, and cohesive energy were calculated. van der Waals ( $\delta_{vdW}$ ) and electrostatic ( $\delta_Q$ ) components of the Hansen solubility parameters were respectively obtained from the square root of the division of the van der Waals (dispersive) and electrostatic contributions of the cohesive energy ( $E_{coh}$ ) by

the molar volume ( $V_m$ ). The total Hansen solubility parameter ( $\delta_H$ ) is then related to the individual components through the formula  $\delta_H^2 = \delta_d^2 + \delta_p^2$ . The hydrogen bond contribution is included in the other terms for OPLS4. The distance between Hansen parameters of different components (Ra) is given by eq 1.<sup>43</sup>

$$Ra^2 = 4(\delta_{vdW,1} - \delta_{vdW,2})^2 + (\delta_{Q,1} - \delta_{Q,2})^2 \quad (1)$$

Energies of mixing ( $\Delta E_{\text{mix}}$ ) in PLA/cellulose and PLA/chitin blends were determined using eq 2, where  $\varphi$  and  $V$ , respectively, stand for the molar composition and volume. A and B stand for the pure systems and AB for PLA/polysaccharide blends, respectively.

$$\Delta E_{\text{mix}} = \varphi_A \left( \frac{E_{\text{coh}}}{V} \right)_A + \varphi_B \left( \frac{E_{\text{coh}}}{V} \right)_B - \left( \frac{E_{\text{coh}}}{V} \right)_{AB} \quad (2)$$

Glass transition temperatures ( $T_g$ ) were estimated by first bringing the polymeric systems to a high temperature (800 K) and then conducting stepwise cooling stages with 10 K intervals and NPT MD simulations being carried out for 5 ns in each stage until 100 K is reached. In each MD stage, we tracked the density changes in each system. At the end of each of them, if the density standard deviation exceeds 5%, an additional 5 ns long NPT MD was performed. We used a 1 fs time step for temperatures higher than 700 K and 2 fs time step for temperatures below that temperature. We used a hyperbolic fit<sup>44</sup> to the density vs temperature curve to identify the high- and low-temperature asymptotes. In this method,  $T_g$  is defined as the temperature at which the intersection of these asymptotes occurs. As described in a previous publication,<sup>32</sup> we opted for this method as it overcomes ambiguities associated with bilinear fits, namely, the selection of the valid ranges for the high- and low-temperature linear zones and allows for easy automated estimation of  $T_g$  values.

Elastic constants were calculated using a stress-based method<sup>42,45</sup> in which successive small strain increments (0.2%) were applied to each structure model's periodic structure followed by 1 ns long Brownian minimizations at 10 K. From a linear fit of the resulting stress as a function of the applied strain, we derived the stiffness matrix of each material. With the assumption of the isotropic structure, we calculated the Young's modulus ( $I$ ), shear modulus ( $G$ ), and Bulk modulus ( $\kappa$ ) from the Lamé constants ( $\lambda$ ,  $\mu$ ) (eqs 3 to 5).<sup>42,46</sup>

$$E = \mu(3\lambda + 2\mu)/(\lambda + \mu) \quad (3)$$

$$G = \mu \quad (4)$$

$$B = \lambda + 2\mu/3 \quad (5)$$

Mechanical strain curves were generated by considering two strain types. A strain type is defined in terms of the parameter  $\eta$ , which relates the transverse strain increment ( $\varepsilon_2$  or  $\varepsilon_3$ ) to the main axis strain increment ( $\varepsilon$ ) by eq 6. In this work, we considered  $\eta$  values corresponding to volume-conserving uniaxial ( $\eta = 0.50$ ) and pure uniaxial ( $\eta = 0.0$ ) tensile loadings with a constant strain rate of  $1.5 \times 10^8 \text{ s}^{-1}$  for each of the three Cartesian axes and then averaged over such axes. For each axis, 200 consecutive steps of 2 ns long NVT MD calculations were performed at 300 K with strain increments of 0.002 ns of the axis length. From the normal component of the stress-strain curves ( $\sigma_{\text{normal}}$ ), we obtained the yield stress ( $\sigma_{\text{yield}}$ ) and

ultimate stress ( $\sigma_{\text{ultimate}}$ ), respectively, defined as the maximum stresses of the elastic and plastic deformation regimes.<sup>46</sup>

$$\varepsilon_2 = 1 + (1 + \varepsilon)^{-\eta} \quad (6)$$

The  $\langle P_2 \rangle$  order parameter was used to identify structural changes in the polymeric models and is defined by eq 7, where  $\theta$  is the angle between a segment vector and the orientation axis of a probe molecule. We used the end-to-end distance ( $h$ ) and radius of gyration ( $R_g$ ) to measure the compactness of the polymer macromolecules. The former is straightforwardly determined from the longest bond path ends, while the latter is calculated from the average squared distance of any polymer atom from its center of mass (eq 8). To measure the stiffness of the polymeric backbone, we calculated the persistence length ( $L_p$ ), the distance over which two points in the polymer chain become decorrelated, and can be calculated by eq 9. In eqs 7–9,  $N$  is the number of atoms in the polymer,  $\mathbf{r}_k$  and  $\mathbf{r}_{\text{mean}}$  are, respectively, the vector of the coordinates of a  $k$ -th atom and the center of mass of the molecule, and  $L_0$  is the extended chain length.

$$\langle P_2 \rangle = \frac{3\langle \cos^2 \theta \rangle - 1}{2} \quad (7)$$

$$R_g^2 = \frac{1}{N} \sum_{k=1}^N (\mathbf{r}_k - \mathbf{r}_{\text{mean}})^2 \quad (8)$$

$$\langle h^2 \rangle = 2L_p L_0 [1 - (L_p/L_0)(1 - \exp(-L_p/L_0))] \quad (9)$$

The location and size of voids in the polymeric structures were determined by a grid-based method where grid points are in a void if they do not fall within the van der Waals radius of any atom plus a probe radius. In this void estimation procedure, grid spacings were defined with a 0.25–1 Å range and a probe radius of 1.40 Å was utilized.

Hydrogen bonds were identified using a geometric criterion where a hydrogen bond is identified when both the distance between a donor (D) and acceptor (A) is less than 3.4 Å and the D–H–A angle is larger than 120°. We calculated the hydrogen bond lifetime in our polymeric systems using a continuous autocorrelation function for the hydrogen bond,<sup>47</sup> as given in eq 10:

$$C(\tau) = \left\langle \frac{h_{ij}(t_0)h_{ij}(t_0 + \tau)}{h_{ij}(t_0)^2} \right\rangle \quad (10)$$

where  $h_{ij}$  is returned a value of 1 or 0, respectively, whether a hydrogen bond occurs between the  $i$ -th and  $j$ -th atoms. The hydrogen bond lifetime ( $\tau_{LT}$ ) is then obtained by fitting a bi-exponential curve to eq 10, as shown in eq 11:

$$\tau_{LT} = A \exp(-t/\tau_1) + B \exp(-t/\tau_2) \quad (11)$$

## RESULTS AND DISCUSSION

**Miscibility and Mutual Organization.** To evaluate the properties of the two PLA/polysaccharide blends studied in this work, we first explored the individual characteristics of each of the polymeric components. Polylactic acid displays interaction patterns considerably different from those shown by polysaccharide molecules. PLA presents a predominance of dispersed forces, as clearly seen in the van der Waals component of the Hansen solubility parameter ( $\delta_H^{\text{PLA}}$ ). On the other hand, cellulose and chitin show a much larger

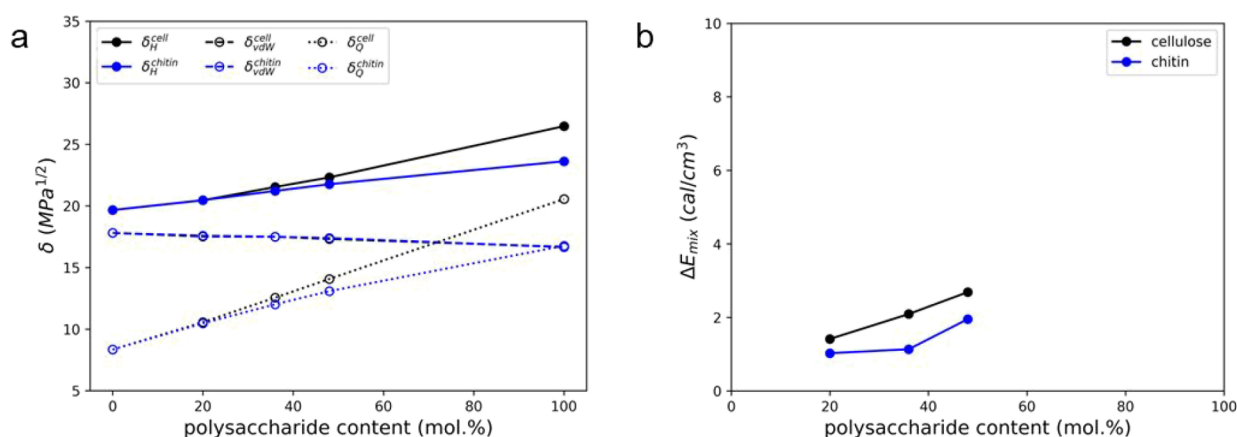


**Figure 2.** Hansen solubility coefficient (solid lines) and its van der Waals (dashed lines) and electrostatic (dotted lines) components obtained from cellulose- (black lines) and chitin-containing (blue lines) PLA blends (a) and energies of mixing of such blends at different polysaccharide contents (b).

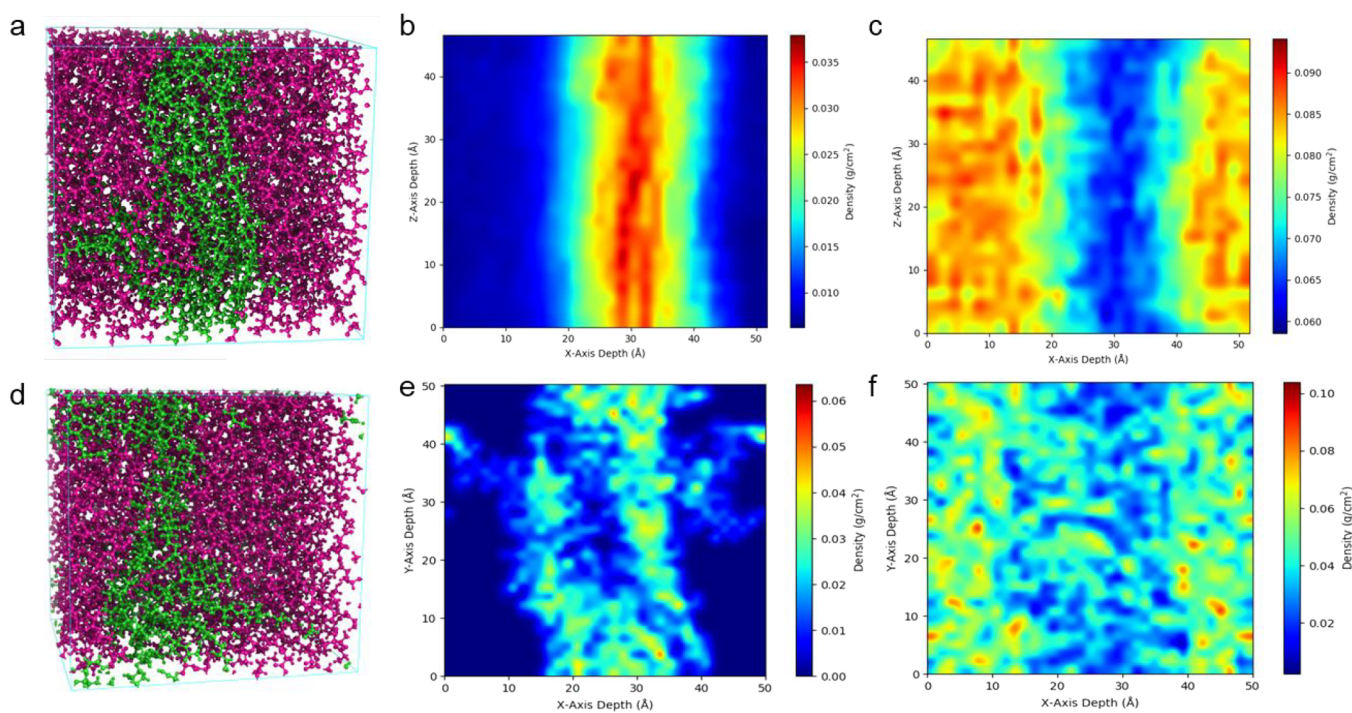


**Figure 3.** Representative snapshots of 20 mol % cellulose- (a) and chitin-containing (d) PLA composites and their respective density heat maps, displaying the density of cellulose (b), chitin (e), and their respectively associated PLA matrices (c,f).

presence of polar interactions, such as those found in hydrogen bonds. This is again clearly seen in their respective solubility parameters ( $\delta_H^{cell}$  and  $\delta_H^{chitin}$ ), which display a predominance of its electrostatic components (cf. Figure 2a). Interestingly, the van der Waals (vdW) component of  $\delta_H^{cell}$  and  $\delta_H^{chitin}$  is similar to the same component of  $\delta_H^{PLA}$ , indicating that the dispersive interaction is similar between the PLA and polysaccharide phases.

When compared to experimental measurements, our calculated  $\delta_H^{PLA}$  values showed varying degrees of agreement. For instance, the  $\delta_H^{PLA}$  value (19.7 MPa<sup>0.5</sup>) matched exactly experimental measurements (19–20.7 MPa<sup>0.5</sup>),<sup>48–50</sup> while  $\delta_H^{cell}$  (26.5 MPa<sup>0.5</sup>) and  $\delta_H^{chitin}$  (23.6 MPa<sup>0.5</sup>) are considerably lower than their corresponding experimental values (29.3 MPa<sup>0.5</sup> and 41.15 MPa<sup>0.5</sup>).<sup>51,52</sup> The discrepancy between calculated and experimental solubility parameters observed in the poly-

saccharide materials can be explained by the inherent crystallinity of typical experimental samples, particularly the polysaccharide components.

Solubility parameters are particularly useful when they are compared with a reference phase. The solubility parameter distance (Ra) is commonly used as a simplified way to quantify the difference in miscibility between two components, where the larger the Ra is, the larger their immiscibility. Knowing that polysaccharides and PLA are well-known experimentally by their mutual immiscibility, we then compared Ra parameters for both cellulose/PLA ( $Ra^{cell} = 12.4 \text{ MPa}^{0.5}$ ) and chitin/PLA ( $Ra^{chitin} = 8.7 \text{ MPa}^{0.5}$ ). This clearly confirms that these polysaccharides are far from being soluble in PLA; however, it also shows that chitin is much closer in miscibility to PLA than cellulose.

Despite the useful trends offered by the analyses of miscibility parameters, they do not provide a full picture of the miscibility in PLA/polysaccharide mixtures. Since these parameters are based on the cohesiveness of pure phases, they do not consider the mutual entropic interactions between these two phases during their mixing. Alternatively, the energy of mixing (eq 2) provides a good picture of the energy penalty related to the mixing of the two polymeric phases considered in this work. As shown in Figure 2b, one can see that the mixing of polysaccharides to PLA is repulsive with energies reaching 1.4–2.7 cal/cm<sup>3</sup> and 1–1.95 kcal/cm<sup>3</sup> for cellulose and chitin. Here, we see again by the lower repulsion energy upon chitin mixing into PLA that this polysaccharide seems to be more compatible with the PLA matrix.

Interestingly, one can notice that the  $\Delta E_{\text{mix}}$  values remain stable at different polysaccharide concentrations. This is an indication that the PLA and polysaccharide components form two distinct phases. Such overall phase segregation in PLA/cellulose and to a lesser degree in PLA/chitin systems is confirmed by tracking the density maps of atoms belonging to each polymeric group, as seen in Figures 3 and S2. This spontaneous nanoscopic scale segregation has been seen experimentally using atomic force microscopy imaging on PLA/cellulose systems,<sup>8</sup> which reveals the nucleation of separate cellulose strands within a PLA matrix.

**Density, Void, and Structural Analyses.** To determine how well our computational methodology can describe the bulk organization of the polymers studied herein, we compared MD-obtained and experimental densities of PLA and the polysaccharides. As shown in Figure 4, one can see that the

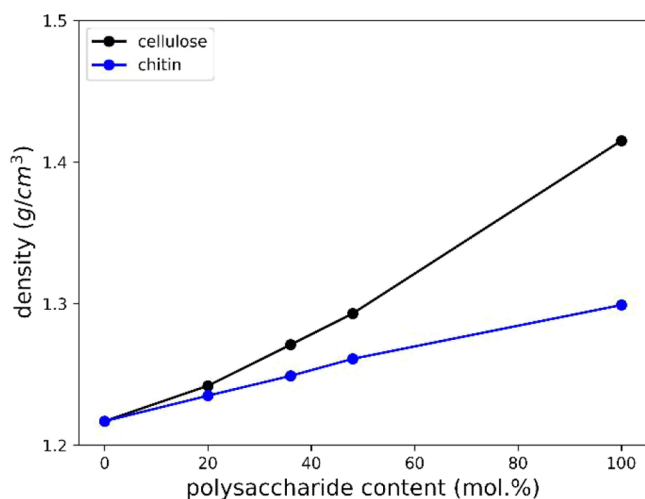


**Figure 4.** Density values of microscopic models of PLA blends with cellulose (black line) and chitin (blue line) at 300 K and 1.013 bar.

calculated PLA density (1.22 g/cm<sup>3</sup>) is quite close to the experimental density value (1.25 g/cm<sup>3</sup>) reported for amorphous PLA.<sup>4,53</sup> A similar agreement is also observed for cellulose, with a calculated density value (1.41 g/cm<sup>3</sup>) close to values usually seen in bulk amorphous cellulose substrates (1.39–1.48 g/cm<sup>3</sup>).<sup>54,55</sup> Since chitin is obtained from organic substrates, it shows different true densities depending on its origin source (1.2–1.4 g/cm<sup>3</sup>).<sup>56</sup> Figure 4 shows that our MD-obtained chitin density (1.30 g/cm<sup>3</sup>) is located within this density range. This, together with a previous benchmark

study,<sup>33</sup> suggests that our model provides a good description of the self-organization of these polymeric materials.

Interestingly, we observed that amorphous polysaccharide macromolecules are re-oriented due to the PLA presence. This can be clearly seen by inspecting the  $\langle P_2 \rangle$  order parameters (cf. Figure 5a) of these molecules, which changes from a stage of a near absence of long-range ordering in their pristine state (in conformity with previous experimental findings)<sup>57,58</sup> toward a more directionally oriented configuration upon increasing concentrations of PLA. However, as we can see by the bimodal distribution profile of  $\langle P_2 \rangle$  order parameters in Figure S3, this reorientation has at least two directions, and there are some portions of polysaccharide molecules not fully aligned in the composites even at the highest PLA concentrations. We attribute this PLA-induced polysaccharide reorientation to both the ineffective PLA/polysaccharide intermolecular bonds and the efficient self-interactions in the polysaccharide phases (vide infra).

As one might expect, this chain reconfiguration greatly affects the extension properties of the carbohydrates. In Figure 5b,c, we can notice that the radius of gyration and end-to-end distance of the carbohydrates increase with larger concentrations of PLA. This is a clear indication that the presence of an adjacent PLA matrix induces the aggregation and linear orientation of the polysaccharide strands. This more linear configuration of polysaccharide molecules when surrounded by a PLA matrix can be verified at the molecular level upon analysis of torsional angles  $\varphi$  and  $\psi$  associated with the glycosidic linkage in both polysaccharides. As seen in Figure S4, the distribution of  $\varphi$  and  $\psi$  is considerably narrower around, respectively,  $-150^\circ$  and  $110^\circ$  when the polysaccharide molecules are embedded in the PLA matrix than in their pristine amorphous state, indicating more linearly organized backbones. Such PLA-induced polysaccharide reorganization positively impacts the rigidity of these molecules, as seen by inspecting the persistence length profiles of Figure 5d.

Similar behavior of polysaccharide molecules within soft polymer matrices has also been observed experimentally.<sup>59</sup> Interestingly, the PLA molecules did not appear to be greatly affected in terms of their self-organization or rigidity in the presence of the polysaccharide molecules. Experimentally, PLA's crystallization was seen to be favored with the presence of cellulose<sup>60</sup> and chitin.<sup>61</sup> However, the lengthy time scales and nucleation barriers involved in such crystallization events, limited their capture in this atomistic molecular dynamics study.<sup>62,63</sup> Given that recently, coarse-grained molecular dynamics calculations were successfully employed to explore the characterization of such crystallization events in pure PLA,<sup>64</sup> future studies extending the use of this computational approach to PLA composites could be of interest.

**Prediction of Mechanical Properties.** After this discussion on the structuring of PLA, polysaccharides, and their composites, we turn our attention to the mechanical properties of these materials. In practical applications, assembling PLA composites has as its primary goal the improvement of tensile-related properties since pristine PLA suffers from, among other issues, small elongation at break and poor impact strength. Since the lengths of the polymers in this study are smaller than the entanglement length,<sup>65</sup> only mechanical properties minimally impacted by the amount of entanglement, moduli, and yield point, are selected for study. Properties highly dependent on entanglement, e.g., strain-

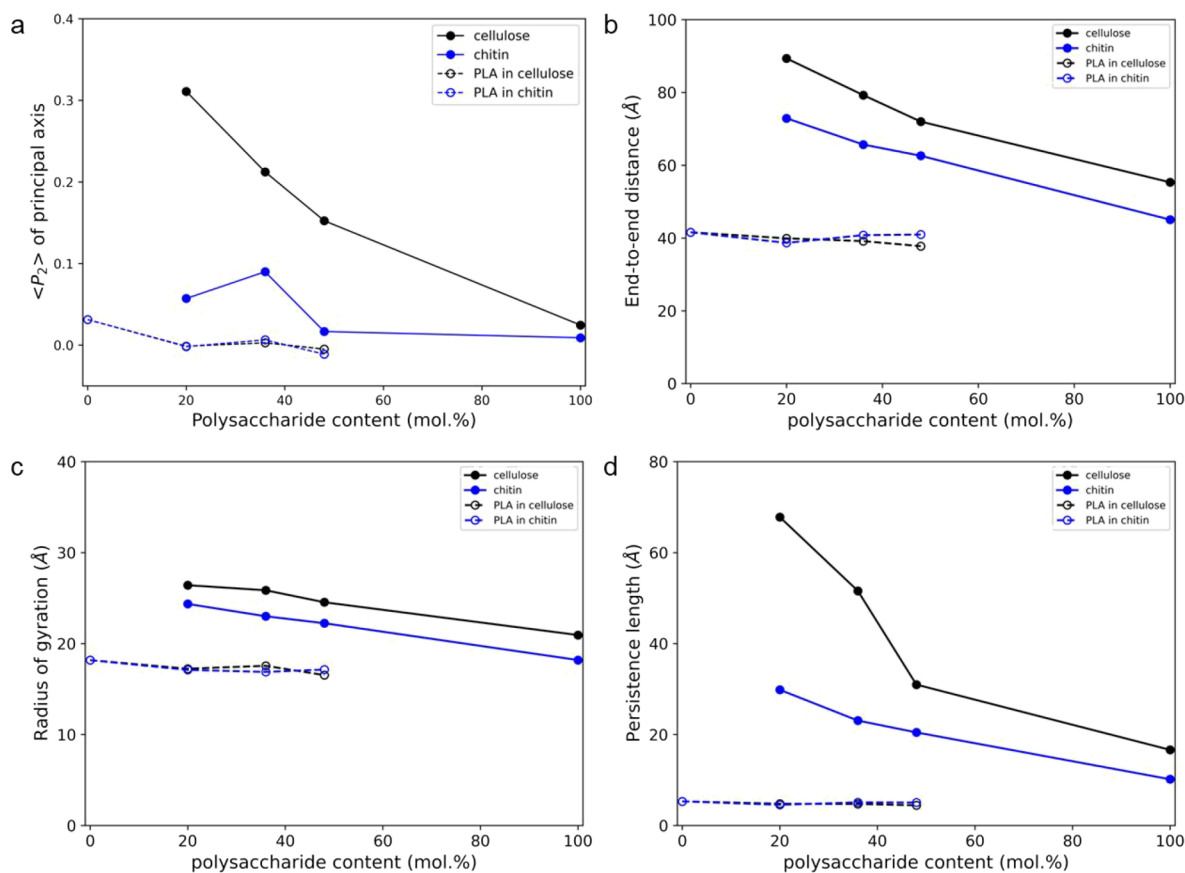


**Figure 5.**  $\langle P_2 \rangle$  order parameter (a), end-to-end distance (b), radius of gyration (c), and persistence length (d) of cellulose and chitin in their pristine state and in blends with PLA (solid lines), as well as corresponding analysis for PLA in its pristine state and in blends with different concentrations of polysaccharides (dashed lines).

hardening behavior, are disregarded as outside the scope of our current models.

Elastic constants are typical properties used to characterize the mechanical properties of polymeric systems. Among them, Young's modulus ( $E$ ) is easily obtained experimentally from tensile tests and therefore frequently measured in polymeric systems. Other related properties such as bulk modulus ( $\kappa$ ) and shear stress ( $B$ ) are less easily measured and more often obtained indirectly.<sup>66</sup> In order to analyze the elastic behavior of our PLA/polysaccharide systems, we constructed elastic tensors as described in the previous section. To validate such a methodology, we initially compared the elastic moduli of both PLA and polysaccharide materials in their pristine state. As seen in Figure 6, the computed  $E$  value for PLA (5.5 GPa) somewhat overestimates the value range typically obtained experimentally at room temperature (3.5–4.1 GPa),<sup>67,68</sup> probably due to the higher strain rates employed in our simulations in comparison with the ones employed experimentally. On the other hand, our in-silico  $E$  values for cellulose (15.1 GPa) are in conformity with the higher range of experimental values obtained for amorphous cellulose (13 GPa)<sup>24,69</sup> and cellulose fibers (10.9 GPa)<sup>70</sup> and somewhat higher than the previous simulated values for amorphous cellulose (10.4 GPa,<sup>42</sup> 14.6 GPa,<sup>71</sup> and 5.6 GPa<sup>29</sup>). The same correspondence was obtained for chitin, whose computed  $E$  value (9.8 GPa) agrees with experimental measurements in chitin films (6.7–8.8 GPa).<sup>72–75</sup> This fundamental difference in tensile strength between chitin and cellulose may be explained by the inherent presence of large void volumes in the

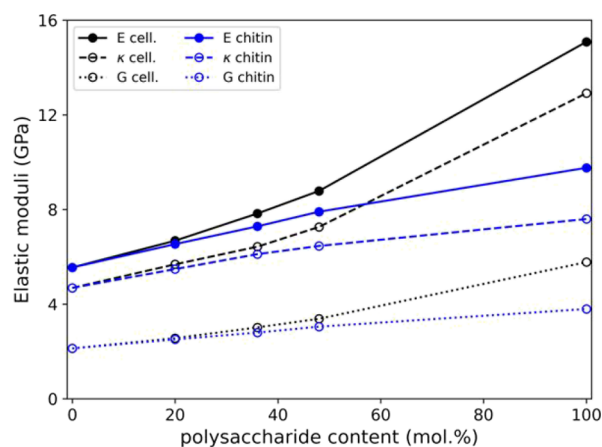


**Figure 6.** Elastic constants obtained from the molecular mechanics workflow: Young's modulus (solid lines), bulk modulus (dashed lines), and shear modulus (dotted lines) of cellulose- (in black) and chitin-containing (in blue) PLA composites and respective pristine materials.

chitin matrix (Figure S5). The presence of larger void zones is indicative of less compact material and therefore more amenable to stress–strain. Moreover, as explained elsewhere,<sup>29</sup> one can also directly correlate the stress properties of a polysaccharide with its hydrogen bond cohesiveness.

As seen in Figure 6, we predict a substantial gain in Young's modulus of the PLA composites with respect to the pristine PLA material. Interestingly, the significant difference observed

between the E values of chitin and cellulose does not translate in equal magnitude to their respective composites with PLA, possibly due to the importance of crossed interactions with the main PLA matrix. We can also note that in our computational predictions, the polysaccharide-containing PLA composites showed a considerable gain in their Young's modulus if compared with the pristine PLA material. Similar trends have been observed experimentally for cellulose- and chitin-containing PLA composites, which showed substantial gains in elastic moduli in comparison with pure PLA.<sup>70,76,77</sup>

Besides the elastic properties, a thorough characterization of the tensile properties of a material requires the evaluation of its ultimate properties, (i.e., yield and ultimate tensile strengths). In this work, we evaluated these properties by generating stress–strain curves considering uniaxial and volume-conserving deformation behavior (see Figure S6).

PLA shows a tensile strength of ca. 63 MPa and an elongation at a break of 1.8%.<sup>68</sup> From our MD-obtained stress–strain profiles, we can see that these characteristics are well captured considering a volume-conserving deformation, where the strain-induced axial elongation is compensated by cross-sectional shrinking. In this configuration, PLA's yield stress ( $\sigma_{\text{yield}} = 79.7$  MPa) and maximum plastic deformation (2.9%) (cf. Figure S6) are on the same order of magnitude as experimental measurements. This is a clear demonstration of the malleable character of PLA.

In comparison with PLA, polysaccharides have, in general, much higher tensile strengths owing to their stronger hydrogen bonds and directional orientation, particularly in their crystalline state. It is difficult to determine single representative values for these materials since they widely depend on their source material, crystallinity degree, and water content.<sup>78,79</sup> For instance, experimental tensile strength in cellulosic materials may vary as much as from 300 MPa to 1 GPa.<sup>78</sup> As seen for the elastic constant values, experimental tensile stresses of amorphous chitin are consistently lower, with values of 270–320 MPa.<sup>74</sup> The simulated values obtained for cellulose ( $\sigma_{\text{yield}} = 391.6$  MPa,  $\sigma_{\text{ultimate}} = 540.9$  MPa), and chitin ( $\sigma_{\text{yield}} = 294.2$  MPa,  $\sigma_{\text{ultimate}} = 451.6$  MPa) (cf. Figure S6) with a pure uniaxial applied strain are in similar ranges as the experimental values. The same applied strain type has been previously used to successfully predict the tensile properties of crystalline<sup>80</sup> and amorphous<sup>42</sup> cellulose. The agreement between experimental and simulated strain values considering pure uniaxial stress in amorphous cellulose and chitin indicates that even in their amorphous state, the tight binding provided by the hydrogen bonds of these polysaccharides would prevent a cross-sectional reordering of the material and favor a purely uniaxial strain pattern. Interestingly, despite such larger stiffness of these polysaccharides in comparison with PLA, they undergo a much experimental larger deformation of ca. 7–8%<sup>42,74</sup> with a clear plastic deformation behavior before their rupture.

This apparent dichotomy of polysaccharides as stiffer yet more deformable than PLA may be explained as a consequence of a polymer chain rigidity/interweaving relationship. As seen in Figure 5d, polysaccharide systems display higher persistence lengths than PLA and are therefore more rigid. More flexible, PLA is more prone to curling between one chain and another and interweaving. Since its cohesiveness is dominated by weak dispersive forces (cf. Figure 2a) PLA would exhibit facile elastic deformation and malleable character that is then closely limited by its further interweaving degree. As discussed elsewhere,<sup>42</sup> the deformation of glucose-based components

until their maximum strain (i.e., 7–8%) is directly associated with the elongation/breaking of hydrogen bonds and increase of relative free volumes. This could be understood as the separation of closely packed (yet not fully interwoven) segments of the polysaccharide macromolecules. Experimentally, larger strains could potentially result in bond cleavage that is not predicted by our molecular models.

The glass transition temperature ( $T_g$ ) is another crucial property of polymeric systems. Usually measured as the center of a transition region from differential scanning calorimetry (DSC) and/or dynamic mechanical analysis (DMA) experiments, the  $T_g$  is characterized by long-range coordinated molecular motions that lead to discontinuities on second-order thermodynamics derivatives (e.g., isobaric heat capacity, thermal expansion coefficient, and isothermal compressibility)<sup>81</sup> of amorphous molecular systems. In Figure S7, we can observe MD-obtained  $T_g$  values for cellulose (525.1 K), chitin (535.9 K), and PLA (401.2 K). Comparing these values with the experimental  $T_g$  values previously obtained for cellulose (493–523 K),<sup>82–84</sup> chitin (335–509 K)<sup>85,86</sup> and PLA (323–343 K),<sup>87–90</sup> one can see that our computed  $T_g$  values are, in varying degrees overestimating the experimental  $T_g$  values. This is a common trend in MD-derived  $T_g$  values for polymeric systems.<sup>32</sup> On the one hand, this likely reflects an MD limitation in reproducing long-range relaxations at cooling rates orders of magnitude faster than the ones experimentally measured. On the other hand, experimental  $T_g$  measurements are also knowingly prone to imprecision related to the partial crystallization of polymer domains or the presence of plasticizing molecules (e.g., water) in the measured samples.<sup>81</sup> Experimental  $T_g$  measurements in polysaccharides are particularly imprecise due to their underlying hydrophilicity, which favors the adsorption of water in their backbone, and their  $T_g$  values being higher than their initial degradation temperatures.<sup>91–93</sup>

We can also observe that the composite PLA models have higher  $T_g$  values than pristine PLA (cf. Figure S7), following an almost linear trend connecting the  $T_g$  of both polymer classes. This linear trend may be associated with the behavior of the two distinct phases contributing to the aggregate density curve such that the total curve is a weight-average. Experimentally, this prediction is not entirely fulfilled. This may be due to the limitation in our microscopic models to represent the macroscopic decorrelation between the immiscible PLA and polysaccharide phases. However, in a recent study,<sup>94</sup> it was shown that while small cellulose contents (up to 5 wt %), indeed induce a slight increase in the composite  $T_g$ , further increase in the cellulose content induced a heterogeneous and cold crystallization of the PLA matrix which resulted in a stagnation and even reduction on the  $T_g$  value in comparison with pristine PLA. This said PLA crystallization is observed both with crystalline and amorphous polysaccharide samples<sup>25</sup> and, together with plasticizing effects exerted by water molecules inherently present in polysaccharide samples, may contribute to a certain extent to the deviation between our predictions and experiments.

**Microscopic Analysis.** Thus far, we have shown that cellulose and chitin behave considerably differently in their pristine state and in the presence of PLA in terms of organization and mechanical properties. Nevertheless, one may wonder about the underlying root cause of this difference. In this section, we scrutinize the microscopic interactions taking place in and between the PLA and polysaccharidic phases

using radial distribution functions (RDFs) and hydrogen bond (HB) analysis. Since we observed in Figure 2a that the van der Waals interactions were practically unaltered with the introduction of polysaccharides into the PLA matrix, we judged the interactions between the polar groups of each polymeric component to be more relevant. In the next paragraphs, we detail the microscopic interactions taking place between the PLA and polysaccharidic phases using radial distribution functions (RDFs) and hydrogen bond (HB) analysis.

The main PLA/polysaccharides interactions occur between PLA's carbonyl (HB acceptor,  $O_{CO}^*$ ) and terminal hydroxyl groups (HB donor,  $O_{OH}^*$ ) and cellulose's hydroxyl groups (HB donor and acceptor,  $O_{OH}$ ) or chitin's hydroxyl (HB donor and acceptor,  $O_{OH}$ )/amide groups (both HB donor,  $N_{NCO}$ , and acceptor,  $O_{NCO}$ ). Due to the predominance of  $O_{CO}^*$  groups in PLA, it is the most relevant to the interactions with the polysaccharide phases. As seen in Figure S8a,b, the hydroxyl groups of both cellulose and chitin interact with the PLA's carbonyl groups by means of unfavorable hydrogen bonds with RDFs of intensity less than 1 and similar donor–acceptor equilibrium distances of ca. 2.9 Å.

Upon inspecting further the hydrogen bonds between PLA and the polysaccharide phases (see Figure 7a,b), we see that

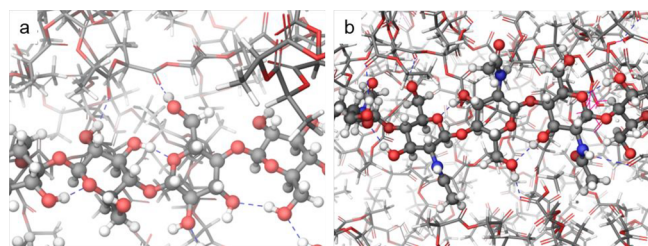


**Figure 7.** Representative snapshots extracted from MD calculations evidencing hydrogen bonds (blue dashed lines) formed among molecules in 20 mol % cellulose-containing (a) and chitin-containing (b) PLA composite structure models. Polysaccharide and PLA molecules are respectively displayed in ball and stick and stick representations. C, O, H, and N atoms are respectively shown in gray, red, white, and blue colors.

the donor groups of cellulose (hydroxyls,  $O_{OH}$ ) and chitin (hydroxyls,  $O_{OH}$ , and the NH portion of the amide groups,  $N_{NCO}$ ) are not particularly engaged in HB bonds with the carbonyl groups of the PLA phase. As seen in Figure 8a, only an average of 0.1 HBs per OH group was observed in cellulose, while in chitin, this value ranges from 0.1 to 0.2 HBs per OH group and from 0.2 to 0.3 HBs per amide group. At the same time, this clearly shows that  $O_{CO}^*$  groups in the main phase are not particularly attractive to the donor groups of the polysaccharides; it also reveals that donor groups in chitin (particularly in the amide groups) are more prone to interact with the PLA phase. It is also noteworthy that these hydrogen bonds become majorly unfavorable upon increasing polysaccharide concentration, as supported by the decrease in their lifetimes ( $\tau_{LT}$ ) upon this condition (cf. Figure 8a).

In analysis of another main hydrogen bond type occurring in PLA/polysaccharide interactions (see Figure 7), we observed terminal  $O_{OH}^*$  groups acting majorly as HB donors while ethers ( $O_{COC}$ ), hydroxyls ( $O_{OH}$ ) and the CO portion of amide groups in chitin ( $O_{NCO}$ ) act as HB acceptors. In this case, upon an increase in the polysaccharide concentration, we see a further

degree of engagement of the  $O_{OH}^*$  groups in HBs with the cellulose and chitin, attaining respective HB/(donor group) values of 0.55 and 0.35 with these components (see Figure 8a). This suggests that enriching the PLA phase with other HB donor components could be a sound strategy to enhance the interaction between PLA and polysaccharide phases. Also interestingly, the effectiveness of these interactions appears to be higher in cellulose than in chitin, since HB lifetimes respectively increase and decrease for the former and latter upon increase of polysaccharide contents (see Figure 8a).

With respect to the interactions within the polysaccharide phases themselves, we inspect the RDFs related to important polar groups, first of all, the mutual interactions between hydroxyl groups. As seen in Figure S9a,b, these interactions have an equilibrium distance of 2.9 Å and are considerably favored upon the decrease in polysaccharide concentration, in conformity with the further degree of ordering of the polysaccharide chains upon PLA addition. In chitin, due to the presence of amide groups, other interactions are also observed. Interactions between hydroxyls and amide groups are quite significant (cf. Figure S10a) and are also promoted upon PLA addition. Intra- and intermolecular self-interactions between amide groups in chitin matrices are also relevant (see Figure S10b) and seem to be reinforced upon reducing chitin content in PLA composites. The efficiency of these interactions is attested by the high intensity of the RDFs associated with them.

Due to the abundance of hydrophilic sites in polysaccharides, hydrogen bonds play a large role in their cohesion. In cellulose, besides the  $\beta$ -glucose's OH (HB donor and acceptor,  $O_{OH}$ ), ether groups (HB acceptor,  $O_{COC}$ ) are also able to participate in HBs (see Figure 7). We observed a number of 0.78 hydrogen bonds per donor group in cellulose (Figure 8b). These hydrogen bonds occur predominantly (79%) among the hydroxyl groups and showed a relatively high average lifetime (ca. 4 ns). Moreover, as seen in Figure 8b, while the presence of PLA induces a marginal decrease in the number of HBs per donor in cellulose, it triggers an increase in the HB lifetime (reaching ca. 5 ns). In chitin, besides hydroxyl and ether groups, amide (NCO) groups also participate in hydrogen bonds both as HB donors (NH) and acceptors (CO). We observed that in chitin, OH groups interact relatively evenly with themselves (0.32 HB/ $O_{OH}$ ), NCO (0.29 HB/ $O_{OH}$ ), and ether groups (0.24 HB/ $O_{OH}$ ), resulting in a slightly higher number of HBs (0.85) per group than in cellulose. On the other hand, NCO interacts much better with OH groups (0.29 HB/NCO) and themselves (0.25 HB/NCO) than with ether groups (0.04 HB/NCO), resulting in a much lower HB count for the group (0.58). Furthermore, as seen in Figure 8b, differently than in cellulose,  $\tau_{LT}$  values in chitin are considerably lower with HBs involving at a time hydroxyl groups or amide groups lasting for, respectively, only 2.7 and 3.5 ns. Both the smaller number of hydrogen bonds per acetyl group and the ephemerality of its hydrogen bonds could explain the less effective chitin's self-reorganization (cf. Figures 3 and 5) in the presence of PLA.

## CONCLUSIONS

We studied PLA associations with cellulose and chitin in terms of their mutual morphology, mechanical properties, and underlying mutual interactions. Our modeling and simulation strategy demonstrated a full-scale reordering of polysaccharide macromolecules upon large PLA concentrations and a reversed

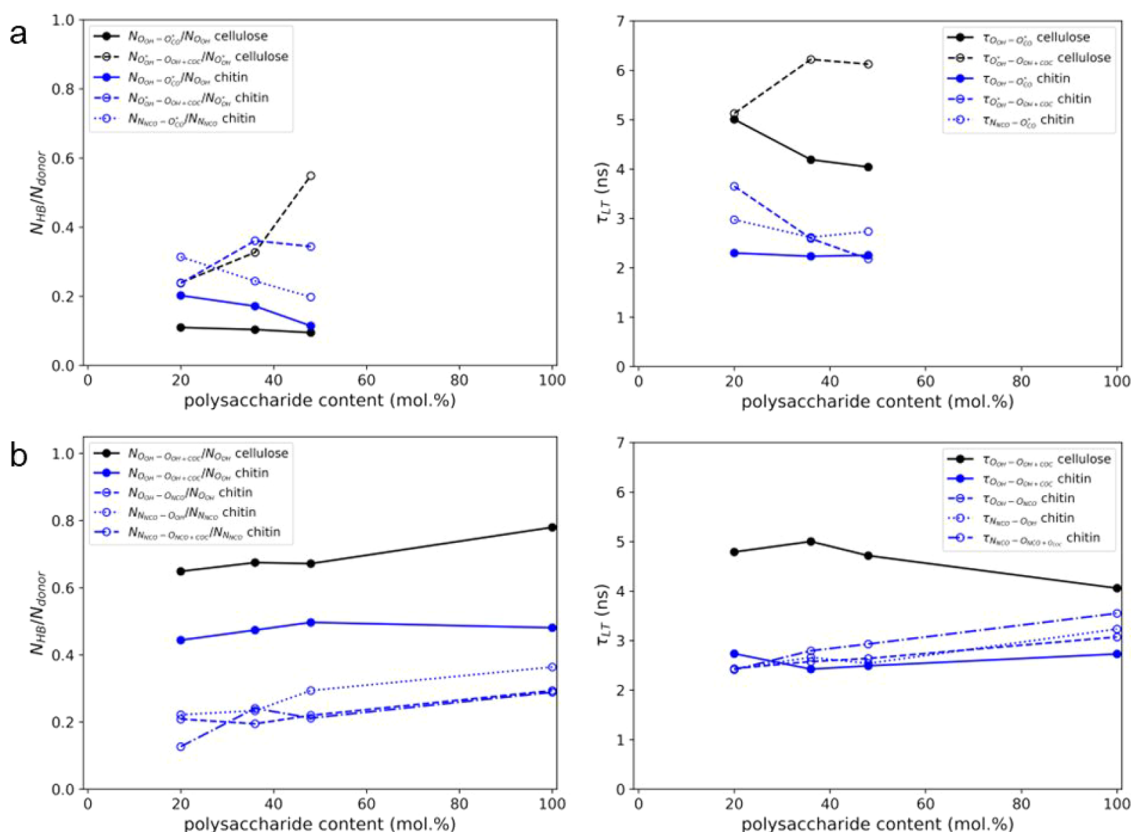


**Figure 8.** Number of hydrogen bonds per donor atom (left) and hydrogen bond average lifetimes (right) (a) between PLA-cellulose (black lines) and PLA-chitin matrices (blue lines) and (b) within cellulose (black curves) and chitin (blue curves) phases.

subtle reorienting of PLA molecules upon polysaccharides. Our structural models were fully validated by their ability to predict thermal, elastic, and stress straining properties of both pristine and composite PLA and polysaccharide materials. Finally, we carried out an extensive nanoscopic analysis of the main interactions taking place in these components, shedding light on the single- and dual-phase interactions between PLA and cellulose or chitin. We expect that these results will offer meaningful insights into the development of higher performing PLA-based biopolymer materials.

## ■ ASSOCIATED CONTENT

### SI Supporting Information

The Supporting Information is available free of charge at <https://pubs.acs.org/doi/10.1021/acsomega.3c04880>.

Miscellaneous information, including heat density maps, stress straining curves, and RDFs (PDF).

## ■ AUTHOR INFORMATION

### Corresponding Authors

Paulo G. M. Mileo – *Schrödinger, GmbH, Mannheim 68163, Germany*; [orcid.org/0000-0002-1363-7268](https://orcid.org/0000-0002-1363-7268);  
Email: [paulo.mileo@schrodinger.com](mailto:paulo.mileo@schrodinger.com)

Andrea R. Browning – *Schrödinger, Inc., Portland, Oregon 97204, United States*; Email: [andrea.browning@schrodinger.com](mailto:andrea.browning@schrodinger.com)

### Authors

Caroline M. Krauter – *Schrödinger, GmbH, Mannheim 68163, Germany*

Jeffrey M. Sanders – *Schrödinger, Inc., New York, New York 10036, United States*; [orcid.org/0000-0003-3279-2850](https://orcid.org/0000-0003-3279-2850)

Mathew D. Halls – *Schrödinger, Inc., San Diego, California 92121, United States*; [orcid.org/0000-0001-8989-8934](https://orcid.org/0000-0001-8989-8934)

Complete contact information is available at:

<https://pubs.acs.org/10.1021/acsomega.3c04880>

## Author Contributions

All authors have given approval to the final version of the manuscript.

## Notes

The authors declare the following competing financial interest(s): All authors are employees of Schrödinger Inc.

## ■ ACKNOWLEDGMENTS

We would like to thank colleagues at Schrödinger Inc for their support and meaningful discussions which contributed to the completion of this work.

## ■ REFERENCES

- Gerassimidou, S.; Martin, O. V.; Chapman, S. P.; Hahladakis, J. N.; Iacovidou, E. Development of an Integrated Sustainability Matrix to Depict Challenges and Trade-Offs of Introducing Bio-Based Plastics in the Food Packaging Value Chain. *J. Cleaner Prod.* **2021**, *286*, No. 125378.
- Vinod, A.; Sanjay, M. R.; Suchart, S.; Jyotishkumar, P. Renewable and Sustainable Biobased Materials: An Assessment on Biofibers, Biofilms, Biopolymers and Biocomposites. *J. Cleaner Prod.* **2020**, *258*, No. 120978.
- Udayakumar, G. P.; Muthusamy, S.; Selvaganesh, B.; Sivarajasekar, N.; Rambabu, K.; Banat, F.; Sivamani, S.; Sivakumar,

- N.; Hosseini-Bandegharai, A.; Show, P. L. Biopolymers and Composites: Properties, Characterization and Their Applications in Food, Medical and Pharmaceutical Industries. *J. Environ. Chem. Eng.* **2021**, *9* (4), No. 105322.
- (4) Farah, S.; Anderson, D. G.; Langer, R. Physical and Mechanical Properties of PLA, and Their Functions in Widespread Applications — A Comprehensive Review. *Adv. Drug Delivery Rev.* **2016**, *107*, 367–392.
- (5) Bezuidenhout, D.; Bouzouita, A.; Brünig, H.; Cain, A.; Chen, X.; Ding, J.; Dubois, P.; Ferrer, G. G.; Groth, T.; Hadasha, W.; Kühnert, I.; Lauro, F.; Li, J.; Liedmann, A.; Liu, J. F.; Liu, T.; Liu, Z.-M.; Malinconico, M.; Niepel, M. S.; Notta-Cuvier, D.; Raquez, J.-M.; Rudolph, N.; Spörer, Y.; Tajitsu, Y.; Tran, N. H. A.; Van den Eynde, M.; Van Puyvelde, P.; Vink, E. T. H.; Yan, L. *Industrial Applications of Poly(Lactic Acid)*; Di Lorenzo, M. L., Androsch, R., Eds.; Springer International Publishing: Cham, 2018; Vol. 282, DOI: 10.1007/978-3-319-75459-8.
- (6) Castro-Aguirre, E.; Iñiguez-Franco, F.; Samsudin, H.; Fang, X.; Auras, R. Poly(Lactic Acid)—Mass Production, Processing, Industrial Applications, and End of Life. *Adv. Drug Delivery Rev.* **2016**, *107*, 333–366.
- (7) Zhao, X.; Hu, H.; Wang, X.; Yu, X.; Zhou, W.; Peng, S. Super Tough Poly(Lactic Acid) Blends: A Comprehensive Review. *RSC Adv.* **2020**, *10* (22), 13316–13368.
- (8) Frone, A. N.; Berlioz, S.; Chailan, J.-F.; Panaitescu, D. M. Morphology and Thermal Properties of PLA–Cellulose Nanofibers Composites. *Carbohydr. Polym.* **2013**, *91* (1), 377–384.
- (9) Mokhena, T.; Sefadi, J.; Sadiku, E.; John, M.; Mochane, M.; Mtibe, A. Thermoplastic Processing of PLA/Cellulose Nanomaterials Composites. *Polymers* **2018**, *10* (12), 1363.
- (10) Mathew, A. P.; Oksman, K.; Sain, M. Mechanical Properties of Biodegradable Composites from Poly Lactic Acid (PLA) and Microcrystalline Cellulose (MCC). *J. Appl. Polym. Sci.* **2005**, *97* (5), 2014–2025.
- (11) Yu, H.-Y.; Zhang, H.; Song, M.-L.; Zhou, Y.; Yao, J.; Ni, Q.-Q. From Cellulose Nanospheres, Nanorods to Nanofibers: Various Aspect Ratio Induced Nucleation/Reinforcing Effects on Poly(lactic acid) for Robust-Barrier Food Packaging. *ACS Appl. Mater. Interfaces* **2017**, *9* (50), 43920–43938.
- (12) Paul, U. C.; Fragouli, D.; Bayer, I. S.; Zych, A.; Athanassiou, A. Effect of Green Plasticizer on the Performance of Microcrystalline Cellulose/Poly(lactic acid) Biocomposites. *ACS Appl. Polym. Mater.* **2021**, *3* (6), 3071–3081.
- (13) Zhou, L.; He, H.; Li, M.; Huang, S.; Mei, C.; Wu, Q. Enhancing Mechanical Properties of Poly(Lactic Acid) through Its in-Situ Crosslinking with Maleic Anhydride-Modified Cellulose Nanocrystals from Cottonseed Hulls. *Ind. Crops Prod.* **2018**, *112*, 449–459.
- (14) Peltzer, M.; Pei, A.; Zhou, Q.; Berglund, L.; Jiménez, A. Surface Modification of Cellulose Nanocrystals by Grafting with Poly(Lactic Acid). *Polym. Int.* **2014**, *63* (6), 1056–1062.
- (15) Martínez de Arenaza, I.; Meaurio, E.; Coto, B.; Sarasua, J.-R. Molecular Dynamics Modelling for the Analysis and Prediction of Miscibility in Poly(lactide)/Poly(vinylphenol) Blends. *Polymer* **2010**, *51* (19), 4431–4438.
- (16) de Arenaza, I. M.; Meaurio, E.; Sarasua, J.-R. Analysis of the Miscibility of Polymer Blends Through Molecular Dynamics Simulations. In *Polymerization*; InTech, 2012, DOI: 10.5772/51327.
- (17) Glova, A. D.; Falkovich, S. G.; Dmitrienko, D. I.; Lyulin, A. V.; Larin, S. V.; Nazarychev, V. M.; Karttunen, M.; Lyulin, S. V. Scale-Dependent Miscibility of Poly(lactide) and Poly(hydroxybutyrate): Molecular Dynamics Simulations. *Macromolecules* **2018**, *51* (2), 552–563.
- (18) Lin, C.; Liu, L.; Liu, Y.; Leng, J. The Compatibility of Poly(lactic acid) and Polybutylene Succinate Blends by Molecular and Mesoscopic Dynamics. *Int. J. Smart Nano Mater.* **2020**, *11* (1), 24–37.
- (19) Wei, Q.; Sun, D.; Zhang, K.; Wang, Y.; Guo, Y.; Wang, Y. Research on the Miscibility, Mechanical Properties and Printability of Poly(lactic acid)/Poly( $\epsilon$ -Caprolactone) Blends: Insights from Molecular Dynamics Simulation and Experiments. *J. Mater. Sci.* **2021**, *56* (16), 9754–9768.
- (20) Takhulee, A.; Takahashi, Y.; Vao-soongnern, V. Molecular Simulation and Experimental Studies of the Miscibility of Poly(lactic acid)/Poly(ethylene glycol) Blends. *J. Polym. Res.* **2017**, *24* (1), 8.
- (21) Ren, Z.; Guo, R.; Bi, H.; Jia, X.; Xu, M.; Cai, L. Interfacial Adhesion of Poly(lactic acid) on Cellulose Surface: A Molecular Dynamics Study. *ACS Appl. Mater. Interfaces* **2020**, *12* (2), 3236–3244.
- (22) Glova, A. D.; Falkovich, S. G.; Larin, S. V.; Mezhskaia, D. A.; Lukasheva, N. V.; Nazarychev, V. M.; Tolmachev, D. A.; Mercurieva, A. A.; Kenny, J. M.; Lyulin, S. V. Poly(Lactic Acid)-Based Nanocomposites Filled with Cellulose Nanocrystals with Modified Surface: All-Atom Molecular Dynamics Simulations. *Polym. Int.* **2016**, *65* (8), 892–898.
- (23) Falkovich, S. G.; Larin, S. V.; Lukasheva, N. V.; Nazarychev, V. M.; Tolmachev, D. A.; Glova, A. D.; Mezhskaia, D. A.; Kenny, J. M.; Lyulin, S. V. Computational Modeling of Poly(lactide) and Its Cellulose-Reinforced Nanocomposites. In *Multifunctional Polymeric Nanocomposites Based on Cellulosic Reinforcements*; Elsevier: 2016; pp 313–341, DOI: 10.1016/B978-0-323-44248-0.00010-9.
- (24) Nishino, T.; Takano, K.; Nakamae, K. Elastic Modulus of the Crystalline Regions of Cellulose Polymorphs. *J. Polym. Sci., Part B: Polym. Phys.* **1995**, *33* (11), 1647–1651.
- (25) Wan Ishak, W. H.; Rosli, N. A.; Ahmad, I. Influence of Amorphous Cellulose on Mechanical, Thermal, and Hydrolytic Degradation of Poly(Lactic Acid) Biocomposites. *Sci. Rep.* **2020**, *10* (1), 11342.
- (26) Ren, Z.; Guo, R.; Zhou, X.; Bi, H.; Jia, X.; Xu, M.; Wang, J.; Cai, L.; Huang, Z. Effect of Amorphous Cellulose on the Deformation Behavior of Cellulose Composites: Molecular Dynamics Simulation. *RSC Adv.* **2021**, *11* (33), 19967–19977.
- (27) Jawalkar, S. S.; Aminabhavi, T. M. Molecular Modeling Simulations and Thermodynamic Approaches to Investigate Compatibility/Incompatibility of Poly(l-lactide) and Poly(vinyl alcohol) Blends. *Polymer* **2006**, *47* (23), 8061–8071.
- (28) Mazeau, K.; Heux, L. Molecular Dynamics Simulations of Bulk Native Crystalline and Amorphous Structures of Cellulose. *J. Phys. Chem. B* **2003**, *107* (10), 2394–2403.
- (29) Kulasinski, K.; Ketten, S.; Churakov, S. V.; Derome, D.; Carmeliet, J. A Comparative Molecular Dynamics Study of Crystalline, Paracrystalline and Amorphous States of Cellulose. *Cellulose* **2014**, *21* (3), 1103–1116, DOI: 10.1007/s10570-014-0213-7.
- (30) *Schrödinger Release 2022–1: Maestro*. Schrödinger, LLC: New York, NY, 2021.
- (31) Lu, C.; Wu, C.; Ghoreishi, D.; Chen, W.; Wang, L.; Damm, W.; Ross, G. A.; Dahlgren, M. K.; Russell, E.; Von Bargen, C. D.; Abel, R.; Friesner, R. A.; Harder, E. D. OPLS4: Improving Force Field Accuracy on Challenging Regimes of Chemical Space. *J. Chem. Theory Comput.* **2021**, *17* (7), 4291–4300.
- (32) Afzal, M. A. F.; Browning, A. R.; Goldberg, A.; Halls, M. D.; Gavartin, J. L.; Morisato, T.; Hughes, T. F.; Giesen, D. J.; Goose, J. E. High-Throughput Molecular Dynamics Simulations and Validation of Thermophysical Properties of Polymers for Various Applications. *ACS Appl. Polym. Mater.* **2021**, *3* (2), 620–630.
- (33) Sanders, J. M.; Misra, M.; Mustard, T. J. L.; Giesen, D. J.; Zhang, T.; Shelley, J.; Halls, M. D. Characterizing Moisture Uptake and Plasticization Effects of Water on Amorphous Amylose Starch Models Using Molecular Dynamics Methods. *Carbohydr. Polym.* **2021**, *252*, No. 117161.
- (34) *Schrödinger Release 2022–1: Desmond Molecular Dynamics System*; D. E. Shaw Research. Maestro-Desmond Interoperability Tools, Schrödinger: New York, NY, 2021.
- (35) Bowers, K. J.; Chow, D. E.; Xu, H.; Dror, R. O.; Eastwood, M. P.; Gregersen, B. A.; Klepeis, J. L.; Kolossvary, I.; Moraes, M. A.; Sacerdoti, F. D.; Salmon, J. K.; Shan, Y.; Shaw, D. E. Scalable Algorithms for Molecular Dynamics Simulations on Commodity

- Clusters. In *SC'06: Proceedings of the 2006 ACM/IEEE Conference on Supercomputing*; 2006; p 43, DOI: 10.1109/SC.2006.54.
- (36) Shaw, D. E.; Grossman, J. P.; Bank, J. A.; Batson, B.; Butts, J. A.; Chao, J. C.; Deneroff, M. M.; Dror, R. O.; Even, A.; Fenton, C. H.; Forte, A.; Gagliardo, J.; Gill, G.; Greskamp, B.; Ho, C. R.; Ierardi, D. J.; Iserovich, L.; Kuskin, J. S.; Larson, R. H.; Layman, T.; Lee, L.-S.; Lerer, A. K.; Li, C.; Killebrew, D.; Mackenzie, K. M.; Mok, S. Y.-H.; Moraes, M. A.; Mueller, R.; Nociolo, L. J.; Peticolas, J. L.; Quan, T.; Ramot, D.; Salmon, J. K.; Scarpazza, D. P.; Schafer, U. Ben; Siddique, N.; Snyder, C. W.; Spengler, J.; Tang, P. T. P.; Theobald, M.; Toma, H.; Towles, B.; Vitale, B.; Wang, S. C.; Young, C. Anton 2: Raising the Bar for Performance and Programmability in a Special-Purpose Molecular Dynamics Supercomputer. In *SC'14: Proceedings of the International Conference for High Performance Computing, Networking, Storage and Analysis*; 2014; pp 41–53, DOI: 10.1109/SC.2014.9.
- (37) Nosé, S. A Unified Formulation of the Constant Temperature Molecular Dynamics Methods. *J. Chem. Phys.* **1984**, *81* (1), 511–519.
- (38) Hoover, W. G. Canonical Dynamics: Equilibrium Phase-Space Distributions. *Phys. Rev. A* **1985**, *31* (3), 1695–1697.
- (39) Martyna, G. J.; Tobias, D. J.; Klein, M. L. Constant Pressure Molecular Dynamics Algorithms. *J. Chem. Phys.* **1994**, *101* (5), 4177–4189.
- (40) Kang, Y.; Zhou, D.; Wu, Q.; Duan, F.; Yao, R.; Cai, K. Fully Atomistic Molecular Dynamics Computation of Physico-Mechanical Properties of PB, PS, and SBS. *Nanomaterials* **2019**, *9* (8), 1088.
- (41) McDonnell, M. T.; Greeley, D. A.; Kit, K. M.; Keffer, D. J. Molecular Dynamics Simulations of Hydration Effects on Solvation, Diffusivity, and Permeability in Chitosan/Chitin Films. *J. Phys. Chem. B* **2016**, *120* (34), 8997–9010.
- (42) Chen, W.; Lickfield, G. C.; Yang, C. Q. Molecular Modeling of Cellulose in Amorphous State. Part I: Model Building and Plastic Deformation Study. *Polymer* **2004**, *45* (3), 1063–1071.
- (43) Hansen, C. M. *The Three Dimensional Solubility Parameter and Solvent Diffusion Coefficient and Their Importance in Surface Coating Formulation*; Technical University of Denmark: Copenhagen, 1967.
- (44) Patrone, P. N.; Dienstfrey, A.; Browning, A. R.; Tucker, S.; Christensen, S. Uncertainty Quantification in Molecular Dynamics Studies of the Glass Transition Temperature. *Polymer* **2016**, *87*, 246–259.
- (45) Fan, C. F.; Hsu, S. L. Application of the Molecular Simulation Technique to Characterize the Structure and Properties of an Aromatic Polysulfone System. 2. Mechanical and Thermal Properties. *Macromolecules* **1992**, *25* (1), 266–270.
- (46) Kaufman, H. S.; Falcetta, J. J. *Introduction to Polymer Science and Technology: An SPE Textbook*; Wiley: New York, 1977.
- (47) Gowers, R. J.; Carbone, P. A Multiscale Approach to Model Hydrogen Bonding: The Case of Polyamide. *J. Chem. Phys.* **2015**, *142* (22), 224907.
- (48) Tsuji, H.; Sumida, K. Poly(L-Lactide): V. Effects of Storage in Swelling Solvents on Physical Properties and Structure of Poly(L-Lactide). *J. Appl. Polym. Sci.* **2001**, *79* (9), 1582–1589.
- (49) Domingues, R. C. C.; Pereira, C. C.; Borges, C. P. Morphological Control and Properties of Poly(Lactic Acid) Hollow Fibers for Biomedical Applications. *J. Appl. Polym. Sci.* **2017**, *134* (47), 45494.
- (50) Ding, Y.; Feng, W.; Huang, D.; Lu, B.; Wang, P.; Wang, G.; Ji, J. Compatibilization of Immiscible PLA-Based Biodegradable Polymer Blends Using Amphiphilic Di-Block Copolymers. *Eur. Polym. J.* **2019**, *118*, 45–52.
- (51) Huu-Phuoc, N.; Nam-Tran, H.; Buchmann, M.; Kesselring, U. W. Experimentally Optimized Determination of the Partial and Total Cohesion Parameters of an Insoluble Polymer (Microcrystalline Cellulose) by Gas-Solid Chromatography. *Int. J. Pharm.* **1987**, *34* (3), 217–223.
- (52) Ravindra, R.; Krovvidi, K. R.; Khan, A. A. Solubility Parameter of Chitin and Chitosan. *Carbohydr. Polym.* **1998**, *36* (2–3), 121–127.
- (53) Auras, R.; Harte, B.; Selke, S. An Overview of Poly(lactides) as Packaging Materials. *Macromol. Biosci.* **2004**, *4* (9), 835–864.
- (54) Sampl, C.; Niegelhell, K.; Reishofer, D.; Resel, R.; Spirk, S.; Hirn, U. Multilayer Density Analysis of Cellulose Thin Films. *Front. Chem.* **2019**, *7*, 251.
- (55) Mark, H. *Encyclopedia of Polymer Science and Technology-Plastics, Resins, Rubbers, Fibers*; Wiley: New York, 1982.
- (56) Al-Hmoud, L.; Abu Fara, D.; Rashid, I.; Chowdhry, B. Z.; Badwan, A. A. Influence of Chitin Source and Polymorphism on Powder Compression and Compaction: Application in Drug Delivery. *Molecules* **2020**, *25* (22), 5269.
- (57) Fink, H.-P.; Philipp, B.; Paul, D.; Serimaa, R.; Paakkari, T. The Structure of Amorphous Cellulose as Revealed by Wide-Angle X-Ray Scattering. *Polymer* **1987**, *28* (8), 1265–1270.
- (58) Kumirska, J.; Czerwicka, M.; Kaczyński, Z.; Bychowska, A.; Brzozowski, K.; Thöming, J.; Stepnowski, P. Application of Spectroscopic Methods for Structural Analysis of Chitin and Chitosan. *Mar. Drugs* **2010**, *8* (5), 1567–1636.
- (59) Saeed, U. Wood Cellulose Fibers Reinforced Polylactic Acid Composite: Mechanical, Thermomechanical Characteristics and Orientation of Fiber. *AIMS Mater. Sci.* **2020**, *7* (1), 9–23.
- (60) Suryanegara, L.; Nakagaito, A. N.; Yano, H. Thermo-Mechanical Properties of Microfibrillated Cellulose-Reinforced Partially Crystallized PLA Composites. *Cellulose* **2010**, *17* (4), 771–778.
- (61) Singh, S.; Patel, M.; Schwendemann, D.; Zacccone, M.; Geng, S.; Maspoeh, M. L.; Oksman, K. Effect of Chitin Nanocrystals on Crystallization and Properties of Poly(Lactic Acid)-Based Nanocomposites. *Polymers* **2020**, *12* (3), 726.
- (62) Karmakar, T.; Invernizzi, M.; Rizzi, V.; Parrinello, M. Collective Variables for the Study of Crystallisation. *Mol. Phys.* **2021**, *119*, 19–20.
- (63) Graham, R. S. Understanding Flow-Induced Crystallization in Polymers: A Perspective on the Role of Molecular Simulations. *J. Rheol.* **2019**, *63* (1), 203–214.
- (64) Ma, B.; Wang, X.; He, Y.; Dong, Z.; Zhang, X.; Chen, X.; Liu, T. Effect of Poly(Lactic Acid) Crystallization on Its Mechanical and Heat Resistance Performances. *Polymer* **2021**, *212*, No. 123280.
- (65) Hoy, R. S.; Robbins, M. O. Strain Hardening of Polymer Glasses: Effect of Entanglement Density, Temperature, and Rate. *J. Polym. Sci., Part B: Polym. Phys.* **2006**, *44* (24), 3487–3500.
- (66) Brown, J. L.; Prime, M. B.; Barton, N. R.; Luscher, D. J.; Burakovsky, L.; Orlikowski, D. Experimental Evaluation of Shear Modulus Scaling of Dynamic Strength at Extreme Pressures. *J. Appl. Phys.* **2020**, *128* (4), No. 045901.
- (67) Torres, J.; Coteló, J.; Karl, J.; Gordon, A. P. Mechanical Property Optimization of FDM PLA in Shear with Multiple Objectives. *JOM* **2015**, *67* (5), 1183–1193.
- (68) Pinto, V. C.; Ramos, T.; Alves, S.; Xavier, J.; Tavares, P.; Moreira, P. M. G. P.; Guedes, R. M. Comparative Failure Analysis of PLA, PLA/GNP and PLA/CNT-COOH Biodegradable Nanocomposites Thin Films. *Procedia Eng.* **2015**, *114*, 635–642.
- (69) Staiger, M. P.; Tucker, N. *Properties and Performance of Natural-Fibre Composites*; Pickering, K. L., Ed.; Woodhead Publishing Limited: 2008.
- (70) Graupner, N.; Herrmann, A. S.; Müssig, J. Natural and Man-Made Cellulose Fibre-Reinforced Poly(Lactic Acid) (PLA) Composites: An Overview about Mechanical Characteristics and Application Areas. *Composites, Part A* **2009**, *40* (6), 810–821.
- (71) Kulasinski, K. *Physical and Mechanical Aspects of Moisture Adsorption in Wood Biopolymers Investigated with Atomistic Simulations*; ETH Zurich: Zurich, 2015.
- (72) Mushi, N. E.; Utsel, S.; Berglund, L. A. Nanostructured Biocomposite Films of High Toughness Based on Native Chitin Nanofibers and Chitosan. *Front. Chem.* **2014**, *2*, 99.
- (73) Butchosa, N.; Brown, C.; Larsson, P. T.; Berglund, L. A.; Bulone, V.; Zhou, Q. Nanocomposites of Bacterial Cellulose Nanofibers and Chitin Nanocrystals: Fabrication, Characterization and Bactericidal Activity. *Green Chem.* **2013**, *15* (12), 3404–3413.

- (74) Wu, Q.; Jungstedt, E.; Šoltéssová, M.; Mushi, N. E.; Berglund, L. A. High Strength Nanostructured Films Based on Well-Preserved  $\beta$ -Chitin Nanofibrils. *Nanoscale* **2019**, *11* (22), 11001–11011.
- (75) Ifuku, S.; Ikuta, A.; Egusa, M.; Kaminaka, H.; Izawa, H.; Morimoto, M.; Saimoto, H. Preparation of High-Strength Transparent Chitosan Film Reinforced with Surface-Deacetylated Chitin Nanofibers. *Carbohydr. Polym.* **2013**, *98* (1), 1198–1202.
- (76) Graupner, N. Application of Lignin as Natural Adhesion Promoter in Cotton Fibre-Reinforced Poly(Lactic Acid) (PLA) Composites. *J. Mater. Sci.* **2008**, *43* (15), 5222–5229.
- (77) Li, J.; Li, J.; Feng, D.; Zhao, J.; Sun, J.; Li, D. Comparative Study on Properties of Polylactic Acid Nanocomposites with Cellulose and Chitin Nanofibers Extracted from Different Raw Materials. *J. Nanomater.* **2017**, *2017*, No. 7193263.
- (78) Jakob, M.; Mahendran, A. R.; Gindl-Altmutter, W.; Bliem, P.; Konnerth, J.; Müller, U.; Veigel, S. The Strength and Stiffness of Oriented Wood and Cellulose-Fibre Materials: A Review. *Prog. Mater. Sci.* **2022**, *125*, No. 100916.
- (79) Hou, J.; Aydemir, B. E.; Dumanli, A. G. Understanding the Structural Diversity of Chitins as a Versatile Biomaterial. *Philos. Trans. R. Soc., A* **2021**, *379* (2206), No. 0331.
- (80) Wu, X.; Moon, R. J.; Martini, A. Tensile Strength of  $I\beta$  Crystalline Cellulose Predicted by Molecular Dynamics Simulation. *Cellulose* **2014**, *21* (4), 2233–2245.
- (81) Cristea, M.; Ionita, D.; Iftime, M. M. Dynamic Mechanical Analysis Investigations of PLA-Based Renewable Materials: How Are They Useful? *Materials* **2020**, *13* (22), 5302.
- (82) Szcześniak, L.; Rachocki, A.; Tritt-Goc, J. Glass Transition Temperature and Thermal Decomposition of Cellulose Powder. *Cellulose* **2008**, *15* (3), 445–451.
- (83) Kalashnik, A. T.; Papkov, S. P.; Rudinskaya, G. V.; Milkova, L. P. Liquid Crystal State of Cellulose. *Polym. Sci.* **1991**, *33* (1), 107–112.
- (84) Goring, D. A. I. Thermal Softening of Lignin, Hemicellulose and Cellulose. *Pulp Paper Mag. Can.* **1963**, *64* (12), T517–T527.
- (85) González-campos, J. B.; Prokhorov, E.; Luna-Bárcenas, G.; Galván, A. M.; Sanchez, I. C.; Nuño Donlucas, S. M.; Garcia-Gaitan, B.; Kovalenko, Y. Relaxations in Chitin: Evidence for a Glass Transition. *J. Polym. Sci., Part B: Polym. Phys.* **2009**, *47* (9), 932–943.
- (86) Kim, S. S.; Kim, S. J.; Moon, Y. D.; Lee, Y. M. Thermal Characteristics of Chitin and Hydroxypropyl Chitin. *Polymer* **1994**, *35* (15), 3212–3216.
- (87) Courgneau, C.; Domenek, S.; Guinault, A.; Avérous, L.; Ducruet, V. Analysis of the Structure-Properties Relationships of Different Multiphase Systems Based on Plasticized Poly(Lactic Acid). *J. Polym. Environ.* **2011**, *19* (2), 362–371.
- (88) Celli, A.; Scandola, M. Thermal Properties and Physical Ageing of Poly (l-Lactic Acid). *Polymer* **1992**, *33* (13), 2699–2703.
- (89) Picciochi, R.; Wang, Y.; Alves, N. M.; Mano, J. F. Glass Transition of Semi-Crystalline PLLA with Different Morphologies as Studied by Dynamic Mechanical Analysis. *Colloid Polym. Sci.* **2007**, *285* (5), 575–580.
- (90) Yu, F.; Liu, T.; Zhao, X.; Yu, X.; Lu, A.; Wang, J. Effects of Talc on the Mechanical and Thermal Properties of Poly(lactide). *J. Appl. Polym. Sci.* **2012**, *125* (S2), E99–E109.
- (91) Moussout, H.; Ahlafi, H.; Aazza, M.; Bourakhouadar, M. Kinetics and Mechanism of the Thermal Degradation of Biopolymers Chitin and Chitosan Using Thermogravimetric Analysis. *Polym. Degrad. Stab.* **2016**, *130*, 1–9.
- (92) Szymańska, E.; Winnicka, K. Stability of Chitosan—A Challenge for Pharmaceutical and Biomedical Applications. *Mar. Drugs* **2015**, *13* (4), 1819–1846.
- (93) Gagić, T.; Perva-Uzunalić, A.; Knez, Ž.; Škerget, M. Hydrothermal Degradation of Cellulose at Temperature from 200 to 300 °C. *Ind. Eng. Chem. Res.* **2018**, *57* (18), 6576–6584.
- (94) Lee, J.-S.; Hwang, G. H.; Kwon, Y. S.; Jeong, Y. G. Impacts of Cellulose Nanofibril and Physical Aging on the Enthalpy Relaxation Behavior and Dynamic Mechanical Thermal Properties of Poly(Lactic Acid) Composite Films. *Polymer* **2020**, *202*, No. 122677.